




Research Paper

^{18}F -DPA-714 PET Imaging for Detecting Neuroinflammation in Rats with Chronic Hepatic Encephalopathy

Xiang Kong¹; Song Luo¹; Jin Rong Wu²; Shawn Wu³; Carlo N. De Cecco⁴; U. Joseph Schoepf⁴; Adam J. Spandorfer⁴; Chun Yan Wang¹; Ying Tian¹; Hui Juan Chen¹; Guang Ming Lu¹; Gui Fen Yang⁵; Long Jiang Zhang¹

1. Department of Medical Imaging, Jinling Hospital, Medical School of Nanjing University, Nanjing, Jiangsu, 210002, China;
2. Department of Pathology, Jinling Hospital, Medical School of Nanjing University, Nanjing, Jiangsu, 210002, China;
3. Medical Imaging Institute of Tianjin, Tianjin, 310092, China;
4. Department of Radiology and Radiological Science, Medical University of South Carolina, Ashley River Tower, MSC 226, 25 Courtenay Dr, Charleston, SC 29401;
5. Department of Nuclear Medicine, Jinling Hospital, Medical School of Nanjing University, Nanjing, Jiangsu, 210002, China.

 Corresponding authors: Long Jiang Zhang, Department of Medical Imaging, Jinling Hospital, Medical School of Nanjing University, Nanjing, Jiangsu, 210002, China. E-mail: kevinzhj@163.com; fax (86) 02580860815. Or Gui Fen Yang, email: nstlygf@163.com.

© Ivyspring International Publisher. Reproduction is permitted for personal, noncommercial use, provided that the article is in whole, unmodified, and properly cited. See <http://ivyspring.com/terms> for terms and conditions.

Received: 2016.02.24; Accepted: 2016.04.19; Published: 2016.05.24

Abstract

Neuroinflammation is considered to be the pathogenesis of hepatic encephalopathy (HE), and imaging neuroinflammation is implicated in HE management. ^{11}C -PK11195, a typical translocator protein (TSPO) radiotracer, is used for imaging neuroinflammation. However, it has inherent limitations, such as short half-life and limited availability. The purpose of this study was to demonstrate the efficiency of new generation TSPO radiotracer, ^{18}F -DPA-714, in detecting and monitoring neuroinflammation of chronic HE. This study was divided into two parts. The first part compared ^{18}F -DPA-714 and ^{11}C -PK11195 radiotracers in ten HE induced rats [bile duct ligation (BDL) and fed hyperammonemic diet (HD)] and 6 control rats. The animal subjects underwent dynamic positron emission tomography (PET) during 2-day intervals. The ^{11}C -PK11195 PET study showed no differences in whole brain average percent injected dose per gram (%ID/g) values at all time points (all $P > 0.05$), while the ^{18}F -DPA-714 PET study showed higher whole brain average %ID/g values in HE rats compared to control group rats at 900 s to 3300 s after injecting radiotracer (all $P < 0.05$). The second part of the study evaluated the effectiveness of ibuprofen (IBU) treatment to chronic HE. Forty rats were classified into six groups, including Sham+normal saline (NS), Sham+IBU, BDL+NS, BDL+HD+NS, BDL+IBU, and BDL+HD+IBU groups. ^{18}F -DPA-714 PET was used to image neuroinflammation. Whole and regional brain average %ID/g values, neurological features, inflammatory factors and activated microglia showed better in the IBU groups than in the NS groups (all $P < 0.05$) and no difference was seen in the Sham groups compared to IBU groups (all $P > 0.05$). In conclusion, this study demonstrated that ^{18}F -DPA-714 is an ideal TSPO radiotracer for imaging neuroinflammation and monitoring anti-neuroinflammation treatment efficacy of chronic HE.

Key words: hepatic encephalopathy, positron emission tomography, neuroinflammation, ibuprofen.

Introduction

Hepatic encephalopathy (HE) is a fatal complication of liver disease that is characterized by a wide range of neuropsychiatric disturbances from

altered mental status to impaired cognitive and decreased motor coordination, that can ultimately progress to stupor and coma [1, 2]. Recent studies

indicated that hyperammonaemia and neuroinflammation have synergistic roles in inducing neurological alterations in HE [1, 3]. Additionally, neuroinflammation has been reported to be involved as an important biomarker for monitoring disease progression in other neurological diseases, such as Alzheimer's disease [4, 5]. Thus, in vivo detection and monitoring of neuroinflammation have important implications in the management of HE and neurological diseases.

Molecular imaging is a potential method for in vivo visualization of neuroinflammation. The 18 kDa translocator protein (TSPO) is an ideal target for neuroinflammation imaging [6, 7]. TSPO is primarily located in the outer mitochondrial membrane. It regulates the transportation of cholesterol into the mitochondria for steroid synthesis. TSPO is also expressed in steroid-synthesizing cells, and is poorly expressed in the brain under healthy conditions [6-8]. Many studies have shown that TSPO expression is upregulated in activated microglial cells in response to inflammation or injury to the brain [6, 9, 10]. Consequently, TSPO may constitute a biomarker of brain inflammation and reactive gliosis. Increased binding of TSPO ligands reflects increased microglia activation, which is a key event of neuroinflammation [11-13]. TSPO expression has been found to be increased in HE animal models, such as those with portacaval shunt (PCS), bile duct ligation (BDL), acute liver failure [14], and even in the brains of patients with cirrhosis who died from hepatic coma [6,15], indicating the role of neuroinflammation in the pathogenesis of HE. Thus, in vivo imaging of TSPO expression can indicate neuroinflammation by using positron emission tomography (PET) with TSPO ligands as molecular imaging agents [6, 7, 10].

¹¹C-PK11195 (¹¹C-N-methyl-N-[1-methylpropyl]-1-[2-chlorophenyl]-isoquinoline-3-carboxamide) was the first developed TSPO radiotracer for neuroinflammation PET imaging, and it has been used in vivo to visualize microglia activation of neuroinflammation [13, 16]. However, ¹¹C-PK11195 has not been widely adopted in clinical applications. The ¹¹C radiotracer is highly lipophilic, resulting in high non-specific binding in the brain and a poor signal-to-noise ratio [11, 17]. Additionally, an on-set cyclotron and essential facilities are needed to work with ¹¹C-PK11195, due to its short half-life and limited availability [11]. Thus, it is necessary to investigate novel radiotracers which have high specific binding in the brain and are clinically practical. Of the developed novel radiotracers, N, N-Diethyl-2-(2-(4-(2-[¹⁸F]fluoroethoxy) phenyl)-5, 7-dimethylpyrazolo [1, 5-a] pyrimidin-3-yl) acetamide (¹⁸F-DPA-714) has a high specificity and binding potential to TSPO and has

already been applied in studying neuroinflammation in many neurological diseases [18-20]. However, the use of ¹⁸F-DPA-714 as a neuroinflammation radiotracer in HE has not been reported.

In this study, we first compared the uptake values of two radiotracers, ¹¹C-PK11195 and ¹⁸F-DPA-714, for in vivo imaging of neuroinflammation in rats with BDL and hyperammonemic diets (HD), which induced hyperammonemia and chronic liver failure to simulate HE [2, 21, 22]. We found that ¹⁸F-DPA-714 might be more suitable for neuroinflammation imaging for chronic HE rats because of significantly statistical difference. Then we used the appropriate radiotracer, ¹⁸F-DPA-714, to investigate the anti-neuroinflammatory treatment efficacy of ibuprofen (IBU) in the chronic HE rats. Accordingly, this study could provide a novel approach for in vivo neuroinflammatory monitoring in chronic HE.

Methods

Subjects

The protocols and procedures were approved by the local Animal Experimental Ethics Committee of Jinling Hospital, Medical School of Nanjing University, Nanjing, China. Fifty-six male Sprague-Dawley rats (180-250 g) [Shanghai Slac Laboratory Animal CO., LTD, Shanghai, China (license number: SCXK (Hu) 2012-0002)] were housed under controlled temperature (20-24°C) and relative humidity (40-70%) conditions with a 12-12 hour light-dark cycle, and fed commercial rat food and tap water. First, two groups were used for the ¹¹C-PK11195 and ¹⁸F-DPA-714 comparison study: Sham group (n =6) and BDL+HD group (n =10). Six groups were involved in the study of ibuprofen (IBU) treatment to HE: Sham + normal saline (NS), Sham+IBU, BDL+NS, BDL+HD+NS, BDL+IBU, and BDL+HD+IBU (n=6 for Sham+NS and Sham+IBU groups, n=7 for other 4 groups).

Bile Duct Ligation

Rats were general anesthetized by using 10% chloral hydrate (Sigma, Missouri, USA) solution injected intraperitoneally in 0.3 ml/100 g of body weight. Under sterile condition, a midline incision was made at upper abdomen, and the common bile duct was segregated, doubly ligated below the bifurcation close to the liver, and served between the two ligatures [2, 21, 22]. Sham group rats were operated in a similar manner except for the bile duct ligation and abscission [2, 21, 22].

Induction of Hyperammonemia

We included the HD group due to the fact that feeding ammonium acetate could increase blood

ammonia and further exacerbate HE conditions [21, 23, 24]. The rats of the HD group were given high concentrate ammonia water daily by intragastric administration in 1 ml/100 g of body weight three weeks after the BDL surgery until their sacrifice [21, 25]. The ammonia water was prepared by dissolving ammonium acetate (Sinopharm Chemical Reagent Co., Ltd, Shanghai, China) in distilled water (50% w/w).

Treatment with Ibuprofen

Rats were treated daily with Ibuprofen (Vetec, Shanghai, China) or saline 10 days after operation and maintained until sacrifice. Ibuprofen in sterile saline was injected intraperitoneally at 30 mg/kg per day in 0.5 ml/100 g of body weight. Control rats were intraperitoneally injected with the same volume of saline [2, 26, 27].

Behavior Studies

Behavior tests were performed before micro-PET scan and all behavior assessments were started at least 1.5 hours after gavage administration and injection of ibuprofen or saline. Rotarod and beam walking tests were used as previously described to evaluate the motor coordination and tolerance of the rats [21, 28]. Locomotor and vertical activity was also assessed with the previously described methods [2, 21, 27, 28]. The detailed methods of these tests can be found in the supplementary materials.

Micro-PET Scans

Twenty-eight days after BDL or sham operation, rats were anaesthetized by isoflurane inhalation (induction: 3% and thereafter 2–2.5%) in oxygen. The radioactive tracers of ^{11}C -PK11195 and ^{18}F -DPA-714 were injected intravenously in the tail vein. ^{11}C -PK11195 [29, 30] and ^{18}F -DPA-714 [19, 31, 32] were synthesized as previously described, the detailed methods can be seen in the supplementary materials. The animals were scanned by an Inveon small animal micro-PET scanner (Siemens Healthcare GmbH, Erlangen, Germany) in prone position. The parameters of micro-PET scan were as follows: slice thickness = 0.78 mm, matrix size = 128 × 128, field of view (FOV) = 4 × 4 cm², energy levels of acquisition: 350 ~ 650 keV [33].

For ^{11}C -PK11195 vs ^{18}F -DPA-714 PET imaging study, 5 rats in the Sham group (one rat had died during surgery) were scanned with ^{11}C -PK11195 first and then ^{18}F -DPA-714 within 48 hrs. In the BDL+HD group, 3 rats had died of severe abdominal infection and liver failure (only one rat underwent ^{11}C -PK11195 PET imaging). Finally, 7 rats were scanned with both ^{11}C -PK11195 and ^{18}F -DPA-714 within 48 hours. Due to the different half-lives of ^{11}C and ^{18}F radiotracers,

micro-PET scans included dynamic and static image acquisition for longitudinal observation. A 30-minute dynamic acquisition was performed after ^{11}C -PK11195 injection and a 10-min static micro-PET scan was performed one hour after ^{11}C -PK11195 injection. Dynamic acquisition with ^{18}F -DPA-714 was performed for one hour after venous injection and the 10-min static ^{18}F -DPA-714 imaging was performed 2 hours after tracer injection. The dynamic acquisition was divided into 6 time points with 5 min interval for ^{11}C -PK11195 PET imaging and 10 min interval for ^{18}F -DPA-714 PET imaging. The mean injected radioactivity of ^{11}C -PK11195 in BDL+HD rats (12.6 ± 1.3 MBq) was not significantly different from Sham rats (10.8 ± 3.5 MBq, $P = 0.209$), while the mean injected radioactivity of ^{18}F -DPA-714 in BDL+HD rats (13.9 ± 1.3 MBq) was not significantly different from Sham rats (15.2 ± 2.5 MBq, $P = 0.288$).

For the IBU treatment study, the rats in Sham+NS ($n = 5$, one rat died of postoperative infection), Sham+IBU ($n = 6$), BDL+NS ($n=6$, one rat did not perform micro-PET scan because of its poor condition), BDL+IBU and BDL+HD+NS ($n = 6$ for each group, one rat died of severe abdominal infection for each group), BDL+HD+IBU ($n = 5$, 2 rats died of severe abdominal infection) groups performed 10-min static PET acquisition at 50 min time point using ^{18}F -DPA-714 based on the above-mentioned study. Based on the shorter imaging time after injecting ^{18}F -DPA-714, we lowered the injected radioactivity in the second part of this study. The mean injected radioactivity of ^{18}F -DPA-714 in all groups was 8.2 ± 1.2 MBq, and there were no differences among six groups ($P = 0.201$).

Image Analysis

^{18}F -DPA-714 data of two rats in BDL+HD and Sham+IBU groups ($n = 1$ for each group) were excluded for marked head motion during imaging acquisition. All images were reconstructed using a three-dimensional ordered-subset expectation maximum algorithm (3D OSEM) after micro-PET acquisition. PMOD 3.0 version software (PMOD Technologies LTD, Zurich, Switzerland) was used to evaluate global and regional brain uptake of radiotracer. The software automatically drew 58 regions of interest (ROI) within the brain avoiding the effect of peripheral vessels and tissues which showed higher tracer distribution, segmented brain regions, and gave the corresponding radioactivity concentration values. The image derived tissue uptake value was obtained by dividing tissue radioactivity with injected dose assuming the tissue density is 1 g/ml, presented as percent injected dose per gram (%ID/g) [20].

Biochemical Characterization

Determination of Plasma Ammonia. One day before micro-PET imaging, rats were deep anesthetized by 10% chloral hydrate (Sigma, Missouri, USA), the canthus blood (0.5~1 mL) was collected to measure venous blood ammonia levels in the morning. After centrifugation at 4500 g for 10 minutes at 4 °C, the supernatants were collected. The supernatants were used to measure ammonia levels by Lambda 35 (PerkinElmer, Massachusetts, USA). Assays were performed on Costar 96-well plates (Corning, New York, USA) [21].

Determination of Liver Function Indicators. The second day after micro-PET scan, blood samples were collected from carotid artery after deep anesthetized by 10% chloral hydrate (Sigma, Missouri, USA). The biochemical indicators of liver function, including alanine aminotransferase (ALT), aspartate transaminase (AST), total proteins, and bilirubin, were measured by correspondent kits (Nanjing Jiancheng Bioengineering Institute, Jiangsu, China) using an autoanalyzer AMS-300 (Beijing Option Science & Technology Development CO., LTD, Beijing, China) [21].

Inflammatory Markers Measurement. The obtained blood samples were collected in Vacutainer tubes containing ethylene diamine tetraacetic acid (EDTA), centrifuged at 400 g for 3 minutes at 4°C, and stored at -80°C until the measurement was conducted. Interleukin (IL)-1 β , IL-6 and tumor necrosis factor alpha (TNF- α) were determined by enzyme-linked immune sorbent assay (ELISA) kits (Abcam, Cambridge, UK) [2, 21].

Histopathologic Examination and Immunohistochemistry

After blood samples were collected, all rats were transcatheterially perfused with 150-200 mL saline, followed by 200 mL phosphate buffered saline (PBS, pH = 7.4) for 20-30 min. Liver and brain specimens were removed and fixed in 10% neutral buffered formaldehyde for 24 hours, and embedded in paraffin. Specimens were then cut to a thickness of 5 μ m using a vibratome. The hematoxylin-eosin (H&E) staining of liver samples was done by the conventional method [22]. For brain immunohistochemistry, free-floating immunohistochemistry was performed as described by previous studies [2, 28]. For staining of microglia, rabbit anti-mouse CD11b antibody (1:500; Abcam, Cambridge, UK) was used as the primary antibody. The secondary antibody was a goat anti-rabbit immunoglobulin G (1:500; Vector, Burlingame, California, USA), which was detected by using the horseradish peroxidase (HRP) method. The detailed method can be found in supplementary

materials. As previously described [1, 2, 5, 21], the typical morphology of resting microglia is ramified, while the activated microglia is transferred into a rod or amoeboid shape. CD11b immunoreactive microglia cells in basal ganglia were quantified according to Rodrigo et al's method [2]. Histo-morphometric analysis was performed with a photomicroscope and digital camera (Olympus IX71, Tokyo, Japan).

Statistical Analysis

Software (SPSS version 16.0; SPSS, Chicago, Ill) was used for statistical analysis. Quantitative data were expressed as mean \pm standard deviation (SD), and the results of each group followed a normal distribution. When only two groups were compared, independent-samples *t*-test was used. Pearson correlation analysis was used to investigate the relationship between systemic inflammatory factors and radiotracer uptake values. Significance between multiple groups was evaluated by one way analysis of variance (ANOVA) followed by a Newman-Keuls post hoc test [2, 21]. *P* value <0.05 was regarded as statistically significant.

Results

Comparative study of ¹¹C-PK11195 and ¹⁸F-DPA-714 micro-PET imaging

Mortality of BDL+HD group animals was 30% (3/10) due to severe abdominal infection. The BDL+HD group rats showed significant liver failure and hyperammonemia compared with controls (Table 1). The level of IL-6 in BDL+HD group was higher than that in Sham group (Table 1). An increase trend of IL-1 β and TNF- α levels in BDL+HD group was seen, however, the difference was not statistically significant (Table 1).

Table 1. Comparison of Biochemical Measurements between Sham and BDL+HD Groups.

Parameters	Sham	BDL+HD	T	P
Plasma ammonia (μ mol/L)	86.5 \pm 16.5	187.0 \pm 36.3	-5.59	0.002**
ALT (KarU)	3.1 \pm 1.0	17.7 \pm 5.2	-6.14	0.003**
AST (KarU)	13.8 \pm 3.2	33.7 \pm 13.4	-3.28	0.028*
Total protein (g/L)	32.9 \pm 3.6	22.9 \pm 4.1	4.72	0.001**
Bilirubin (μ mol/L)	8.0 \pm 0.8	15.6 \pm 2.5	-7.13	<0.001***
IL-1 β (pg/ml)	874.0 \pm 44.3	1170.05 \pm 309.5	-1.89	0.107
IL-6 (pg/ml)	46.9 \pm 2.2	54.3 \pm 2.9	-4.45	0.003**
TNF- α (pg/ml)	98.6 \pm 10.7	121.29 \pm 25.4	-2.01	0.086

Note: Values are the mean \pm standard deviation from at least 4 rats per group. BDL=bile duct ligation; HD=hyperammonemic diet; ALT=alanine aminotransferase; AST=aspartate transaminase; IL=interleukin; TNF- α =tumor necrosis factor alpha.

* P<0.05, ** P<0.01, and *** P<0.001 are regarded as statistically significant.

The behavior studies showed the rats of BDL+HD group had significant impairment of motor activity, coordination and tolerance (Figure 1). The rats of the Sham group stayed on the rotarod longer than BDL+HD group (Figure 1A). The time to cross the beam and number of foot faults of BDL+HD rats were significantly higher compared to the Sham rats (Figure 1B), while crossovers and rearing numbers in the chamber within 15 min for BDL+HD rats were significantly lower compared to the Sham rats (Figure 1C), indicating the impairment of spontaneous motor activity in a new environment for BDL+HD rats.

The global brain uptake values of ^{11}C -PK11195 in BDL+HD rats were not significantly different from Sham rats at all time points (all $P > 0.05$) (Figure 2A, Supplementary Table S1). Thus, ^{11}C -PK11195 was not further investigated in the second section of this study. Global brain uptake values of ^{18}F -DPA-714 in BDL+HD rats were significantly higher than Sham rats at 900 s, 1500 s, 2100 s, 2700 s, and 3300 s time points (all $P < 0.05$) (Figure 2B, Supplementary Table

S2). ^{18}F -DPA-714 radioactivity was attenuated rapidly in the early stage of dynamic acquisition and ^{18}F -DPA-714 uptake at 2700 s and 3300 s trended toward stability (Figure 2B), therefore we chose the data at time points 2700 s and 3300 s to analyze ^{18}F -DPA-714 uptake in regional brain areas. At the two time points, multiple brain regions in BDL+HD group showed higher ^{18}F -DPA-714 uptake values than the Sham group (all $P < 0.05$), including the bilateral basal ganglia, cingulate cortex, hippocampus, somatosensory cortex, thalamus, midbrain, cerebellum, pons, and medulla (Figure 3, Supplementary Table S3). The uptake values at 2700 s and 3300 s time points after intravenous administration of ^{18}F -DPA-714 showed positive correlation with the IL-1 β ($r = 0.808$ and 0.721 , $P = 0.015$ and 0.044 , respectively), IL-6 ($r = 0.924$ and 0.870 , $P < 0.001$ and $P = 0.002$, respectively), and TNF- α levels ($r = 0.760$ and 0.716 , $P = 0.011$ and 0.020 , respectively).

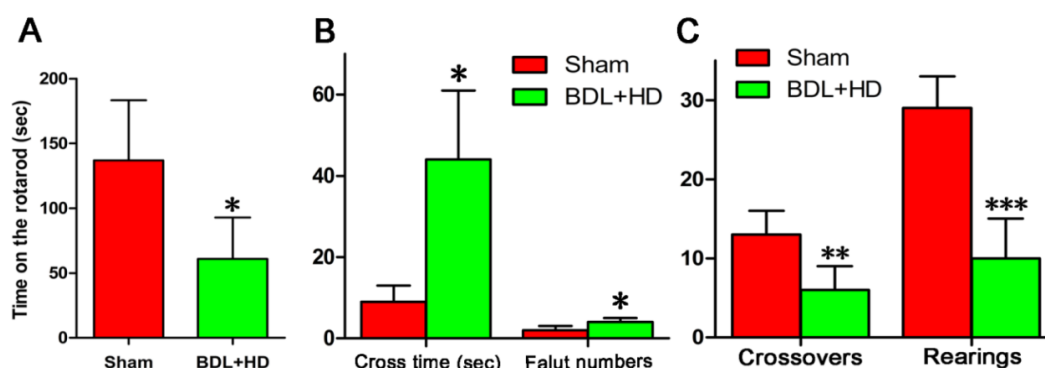


Figure 1. Behavioral tests results in Sham group and BDL+HD group. Rotarod (A), beam walking (B), and motor activity (C) tests show that the values are significantly different from Sham rats. All behavioral test results show significant difference between the two groups. * $P < 0.05$, ** $P < 0.01$, *** $P < 0.001$. BDL=bile duct ligation; HD=hyperammonemic diet.

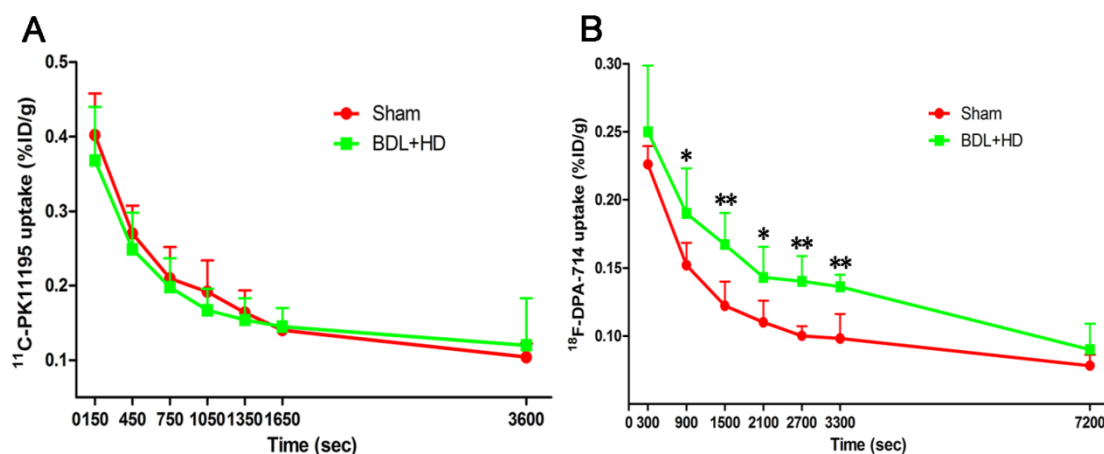


Figure 2. Time activity curves of ^{11}C -PK11195 (A) and ^{18}F -DPA-714 (B) in global brain, expressed as %ID/g of tissue. ^{11}C -PK11195 uptake values show no significant difference between the two groups, while ^{18}F -DPA-714 uptake values in BDL+HD rats were higher than Sham rats at 900 s, 1500 s, 2100 s, 2700 s, and 3300 s time points. * $P < 0.05$, ** $P < 0.01$. BDL=bile duct ligation; HD=hyperammonemic diet.

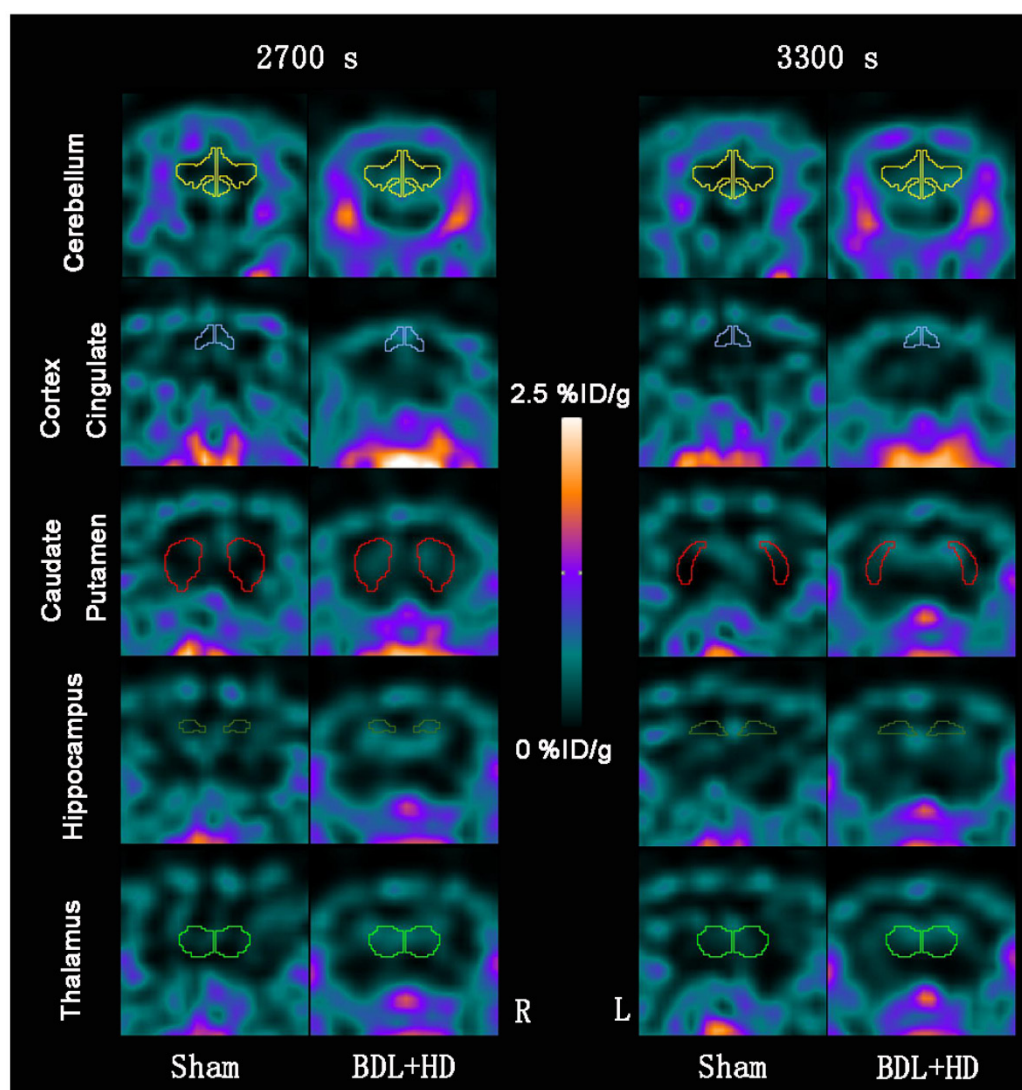


Figure 3. Representative ^{18}F -DPA-714 micro-PET images of several regional brain regions at 2700 s and 3300 s time points between Sham and BDL+HD groups. Representative micro-PET images at 2700 s and 3300 s time points in cerebellum, cortex cingulate, caudate putamen, hippocampus, and thalamus show that Sham operated rats have lower ^{18}F -DPA-714 uptake values (%ID/g) than BDL+HD rats. BDL=bile duct ligation; HD=hyperammonemic diet; L=left; R=right.

After more than 28 days post-surgery, the liver weight of BDL+HD rats (24 ± 5 g) was significantly heavier than Sham rats (14 ± 4 g, $P = 0.010$), indicating that the livers after BDL surgery were compensatory hyperplasia (Supplementary Figure S1A). The liver H&E staining revealed the evidence of biliary cirrhosis in BDL+HD rats (Supplementary Figures S1B and S1C). CD11b immunohistochemistry analysis of microglia showed the microglial cells of basal ganglia, hippocampus, thalamus, and cerebellum in Sham rats were ramified, which is the typical morphology of resting microglia (Supplementary Figure S2A). While in BDL+HD rats, the microglia in these brain regions showed amoeboid shapes, suggesting that the microglia had been activated for neuroinflammation (Supplementary Figure S2B). It was also noted that the amount of CD11b immunoreactive microglia in the basal ganglia of

BDL+HD rats was 16.0 ± 4.1 cells/ mm^2 , which was significantly higher compared to Sham rats (10.0 ± 1.9 cells/ mm^2 , $P < 0.01$).

^{18}F -DPA-714 micro-PET imaging of ibuprofen treatment to chronic HE

The mortality rate of IBU treated BDL and BDL+HD rats was 21% (3/14) higher than the mortality rate of NS treated BDL and BDL+HD rats (7%, 1/14), which can be explained by severe abdominal infection rather than HE. Although IBU did not affect blood ammonia level in HE rats, IL-6 and TNF- α levels showed significant difference between each group (Table 2), indicating that IBU could inhibit the expression and release of inflammatory factors.

Behavioral studies showed statistical difference among 6 groups (all $P < 0.01$), while no significant

differences were observed between Sham+NS and Sham+IBU rats, between BDL+NS and BDL+HD+NS rats, and between BDL+IBU and BDL+HD+IBU rats (all $P > 0.05$) (Figure 4). IBU treated rats also showed no significant differences for behavioral studies compared to Sham operated rats, while NS treated BDL and BDL+HD rats were significantly different from IBU treated rats and Sham operated rats (Figure 4). These results indicated that IBU treatment could restore motor function of chronic HE rats including motor activity, motor coordination, and tolerance.

^{18}F -DPA-714 was used to evaluate the IBU treatment efficacy of neuroinflammation in chronic HE. This study showed that no significant difference was found for global brain uptake values at 3000 s time point between Sham+NS and Sham+IBU groups and between BDL+NS and BDL+HD+NS groups ($P = 0.557$ and 0.788 , respectively) (Figure 5A,

Supplementary Table S4). NS treated rats had the same level of global brain radiotracer uptake values as control rats. Both IBU treated BDL and BDL+HD rats showed lower uptake values than the NS treated and control rats, while BDL+IBU rats showed lower global brain radiotracer uptake values compared to the BDL+HD+IBU rats ($P = 0.016$) (Figure 5A, Supplementary Table S4). In the regional brain comparison, average %ID/g values of multiple regional brain areas including bilateral basal ganglia, cingulate cortex, motor cortex, somatosensory cortex, auditory and visual cortex, hippocampus, thalamus, midbrain, and cerebellum grey matter had significant differences among each group (all $P < 0.01$). Average %ID/g values of these brain regions in IBU treatment groups were lower than those of NS treatment groups, and were similar as those of Sham groups (Figure 5B, Supplementary Table S4).

Table 2. Comparison of Biochemical and Histopathological Measurements among 6 Groups.

Parameters	Sham+NS	Sham+IBU	BDL+NS	BDL+HD+NS	BDL+IBU	BDL+HD+IBU	F	P
Plasma ammonia ($\mu\text{mol/L}$)	78.0 \pm 14.3 ^{cc dd ee}	77.1 \pm 15.3 ^{cc dd ee}	137.7 \pm 24.0 ^{aa bb c d}	199.4 \pm 41.8 ^{aa bb}	149.4 \pm 8.8 ^{aa bb d}	202.5 \pm 33.1 ^{aa bb e}	30.64	<0.001***
ALT (KarU)	6.4 \pm 0.7 ^{cc dd ee}	6.9 \pm 1.4 ^{cc dd ee}	12.5 \pm 3.7 ^{aa bb}	13.5 \pm 3.3 ^{aa bb}	13.2 \pm 4.6 ^{aa bb}	12.9 \pm 3.1 ^{aa bb}	7.39	<0.001***
AST (KarU)	15.0 \pm 3.5 ^{cc dd e}	16.9 \pm 5.7 ^{cc dd}	28.7 \pm 6.8 ^{aa b}	36.5 \pm 15.8 ^{aa bb}	27.9 \pm 4.2 ^a	37.9 \pm 7.4 ^{aa bb}	6.76	<0.001***
Total protein (g/L)	33.4 \pm 3.7 ^{cc dd ee}	35.7 \pm 5.6 ^{cc dd ee}	22.1 \pm 3.1 ^{aa bb}	24.5 \pm 1.9 ^{aa bb}	24.5 \pm 2.8 ^{aa bb}	22.5 \pm 4.1 ^{aa bb}	16.78	<0.001***
Bilirubin ($\mu\text{mol/L}$)	8.1 \pm 1.1 ^e	5.0 \pm 2.1 ^{c d ee}	19.5 \pm 3.9 ^b	26.6 \pm 11.0 ^b	23.2 \pm 5.6 ^{aa bb}	20.0 \pm 5.7 ^b	11.93	<0.001***
IL-1 β (pg/ml)	894.3 \pm 25.4	829.1 \pm 132.3	1135.9 \pm 264.8	1255.3 \pm 365.6	930.8 \pm 122.7	979.4 \pm 253.1	1.68	0.184
IL-6 (pg/ml)	48.1 \pm 1.8 ^{cc}	44.9 \pm 3.0 ^{cc}	51.1 \pm 2.2 ^{bb e}	54.1 \pm 4.3 ^{aa bb dd ee}	46.1 \pm 2.7 ^{cc}	47.9 \pm 1.1 ^{cc}	6.27	0.002**
TNF- α (pg/ml)	95.1 \pm 14.1 ^c	91.6 \pm 17.6 ^{cc}	116.7 \pm 14.8	132.4 \pm 24.6 ^{aa bb e d}	99.8 \pm 11.0 ^c	99.0 \pm 13.9 ^c	3.26	0.032'
No. of microglia (cells/mm ²) &	12.5 \pm 2.7 ^{cc}	11.5 \pm 3.1 ^{cc}	18.1 \pm 4.1 ^{aa bb dd ee}	19.6 \pm 4.6 ^{aa bb dd ee}	12.3 \pm 2.5 ^{cc}	11.8 \pm 3.7 ^{cc}	20.45	<0.001***

Note: Values are the mean \pm standard deviation from at least 4 rats per group.

BDL, bile duct ligation; HD, hyperammonemic diet; NS, normal saline; IBU, ibuprofen; ALT, alanine aminotransferase; AST, aspartate transaminase; IL, interleukin; TNF- α , tumor necrosis factor alpha.

* $P < 0.05$, ** $P < 0.01$, and *** $P < 0.001$ were regarded as statistically significant. Values significantly different from Sham+NS rats are indicated by 'a', from Sham+IBU rats by 'b', from BDL+HD+NS rats by 'c', from BDL+HD+IBU rats by 'd', and from BDL+IBU rats by 'e'. ^a $P < 0.05$; ^{aa} $P < 0.01$; ^b $P < 0.05$; ^{bb} $P < 0.01$; ^c $P < 0.05$; ^{cc} $P < 0.01$; ^d $P < 0.05$; ^{dd} $P < 0.01$; ^e $P < 0.05$; ^{ee} $P < 0.01$.

&, CD11b-positive microglia cells were counted in the basal ganglia.

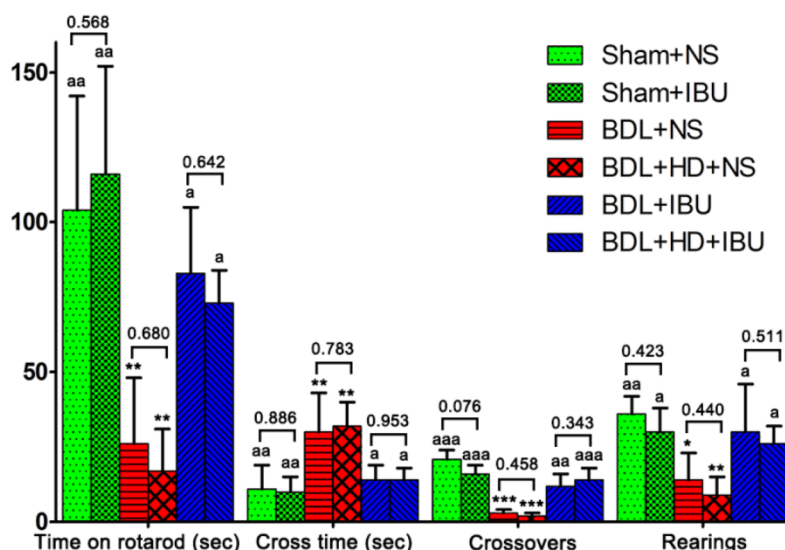


Figure 4. The comparison of rotarod, beam walking, and motor activity tests results among six groups. The comparisons between Sham+NS and Sham+IBU groups, between BDL+NS and BDL+HD+NS groups, and between BDL+IBU and BDL+HD+IBU groups show no significant difference. IBU treated rats show no difference from Sham rats, while NS treated rats show significant difference from Sham and IBU treated rats. * $P < 0.05$, ** $P < 0.01$, and *** $P < 0.001$ for difference from Sham+NS and Sham+IBU groups. ^a $P < 0.05$, ^{aa} $P < 0.01$, and ^{aaa} $P < 0.001$ for difference from BDL+NS and BDL+HD+NS groups. BDL=bile duct ligation; HD=hyperammonemic diet; NS=normal saline; IBU=ibuprofen.

Liver weight of IBU treated BDL (27 ± 6 g) and BDL+HD (26 ± 4 g) rats was heavier than that of Sham+NS (14 ± 2 g) and Sham+IBU (15 ± 1 g) rats (all $P < 0.01$), and was similar to NS treated BDL (25 ± 7 g) and BDL+HD rats (26 ± 5 g) (all $P > 0.05$). Liver H&E staining of IBU treatment rats showed similar findings of NS treatment rats, characterized by the evidence of biliary cirrhosis, while the Sham operated rats showed normal liver pathological characteristics. These findings indicated that IBU treatment did not affect the process of chronic liver failure. However, the morphological analysis of microglia from

immunohistochemistry stained by CD11b showed that the microglia of the IBU treated BDL and BDL+HD rats as well as Sham+NS and Sham+IBU rats were ramified (resting), while the BDL+NS and BDL+HD+NS rats, not treated with IBU, showed typical morphological shape of activated microglia (ameboid), indicating that IBU had a notable anti-neuroinflammation effect in HE (Figure 6). CD11b immunoreactive microglia cells in the basal ganglia of BDL+NS and BDL+HD+NS rats were significantly higher compared to other groups (Table 2). This was consistent with the ^{18}F -DPA-714 findings.

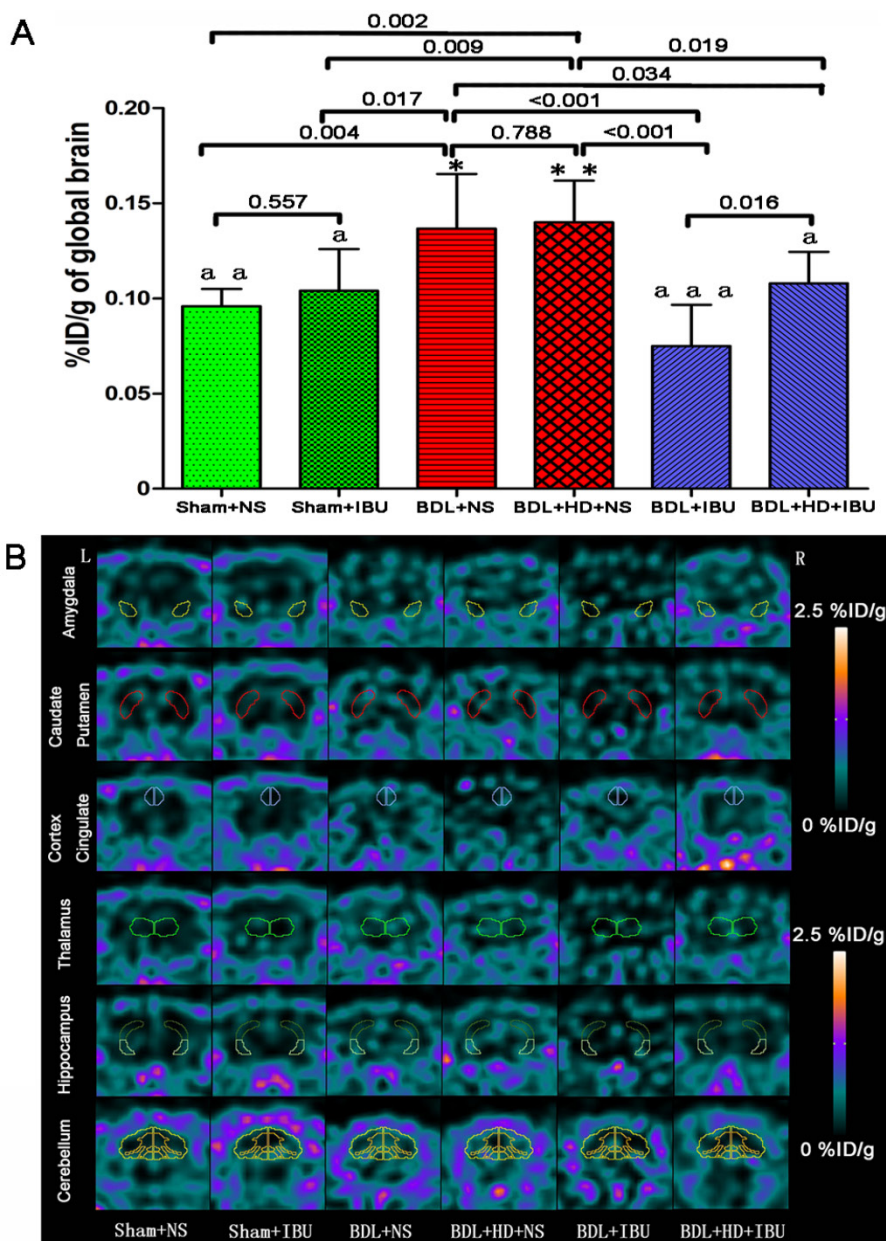


Figure 5. The comparison of ^{18}F -DPA-714 uptake values (%ID/g) of global brain and regional brain regions in six groups. (A) The histogram shows no significant difference between Sham+NS and Sham+IBU groups, and between BDL+NS and BDL+HD+NS groups. BDL+IBU rats showed lower global brain radiotracer uptake values than BDL+HD+IBU rats, and both IBU treated BDL and BDL+HD rats showed lower uptake values than NS treated rats, which had the same uptake values as control rats. * $P < 0.05$ and ** $P < 0.01$ for difference between Sham+NS and Sham+IBU groups. ^a $P < 0.05$, ^{aa} $P < 0.01$, and ^{aaa} $P < 0.001$ for difference between BDL+NS and BDL+HD+NS groups. Representative ^{18}F -DPA-714 micro-PET images of several regional brain regions **(B)** show that IBU treated in BDL and BDL+HD rats have lower ^{18}F -DPA-714 uptake values than NS treated BDL and BDL+HD rats and Sham operated rats. BDL=bile duct ligation; HD=hyperammonemic diet; NS=normal saline; IBU= ibuprofen; L=left; R=right.

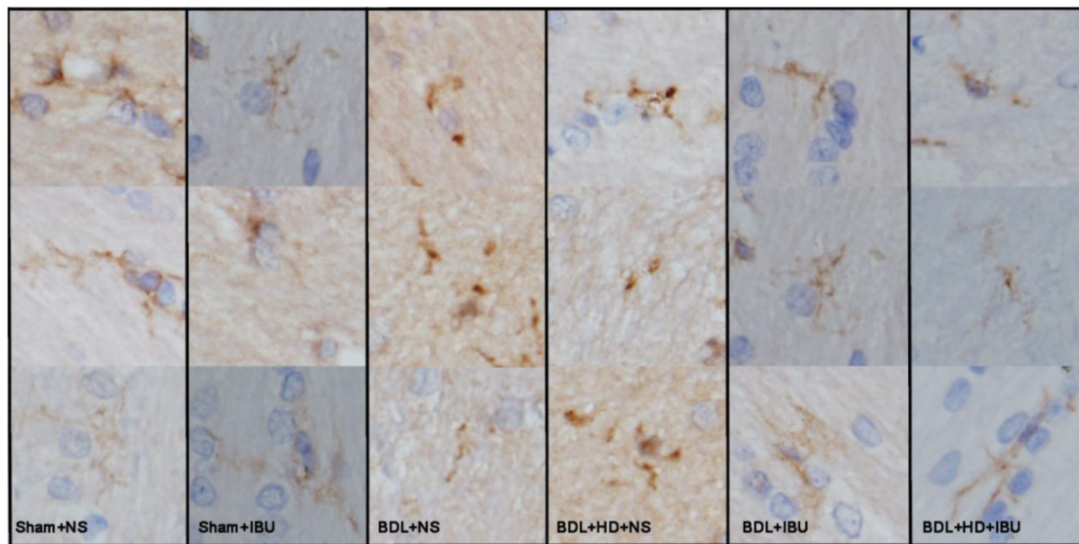


Figure 6. The representative micrographs showing the microglia by CD11b immunohistochemistry of the basal ganglia sections in six groups. Sham operated rats and IBU treated BDL and BDL+HD rats show ramified resting microglia. The NS treated BDL and BDL+HD rats show typical morphological changes of activated microglia (ameboid). BDL=bile duct ligation; HD=hyperammonemic diet; NS=normal saline; IBU=ibuprofen.

Discussion

Neuroinflammation is gaining increased attention in the study of pathogenesis of central nervous system diseases [4, 5], which in recent years has provided new insight for chronic HE [1, 3]. It raises a challenge to search for an effective noninvasive imaging method to monitor neuroinflammation progression and evaluate its response to therapy. PET imaging with different radiotracers targeting TSPO expression in activated microglia has been used to identify neuroinflammation in various central nervous system diseases [7, 10]. ^{11}C -PK11195 PET has been used to image neuroinflammation in HE [13]. However, due to inherent limitations of ^{11}C isotope, ^{18}F -DPA-714 has shown greater promise as a more reliable alternative for PET imaging of TSPO with high specificity and binding potential [18, 19]. Our study compared the imaging ability of ^{11}C -PK11195 and ^{18}F -DPA-714 of neuroinflammation in HE induced rats, and assessed the efficacy of IBU treatment, which is considered to reduce neuroinflammation by its anti-inflammatory effect [2, 26, 27]. Our results showed that ^{18}F -DPA-714 had an improved ability to image neuroinflammation compared to ^{11}C -PK11195 because of highly lipophilic and non-specific binding in the brain for ^{11}C -PK11195 [11, 17] or ^{11}C -PK11195 might be not suitable for chronic HE rats. The other possible explanations for invalidation of ^{11}C -PK11195 were the HE severity and small sample size in our study. ^{18}F -DPA-714 PET can effectively quantify and monitor the treatment response to neuroinflammation in chronic liver failure and hyperammonemia rats [18-20]. Thus, ^{18}F -DPA-714

PET imaging can provide a useful biomarker for evaluating neuroinflammation in chronic HE.

In this study, we found that ^{11}C -PK11195 global brain uptake values are not significantly different between BDL+HD rats and Sham rats, suggesting ^{11}C -PK11195 might not be suitable for neuroinflammation imaging of chronic HE. Our findings were inconsistent with one previous study. Cagnin et al [13] reported that increased cerebral binding of ^{11}C -PK11195 in the bilateral pallidum, right putamen, and right dorsolateral prefrontal cortex in minimal HE patients (n=5) reflected the microglia cell state alterations that may contribute to impaired brain function. However, the small sample with heterogeneous etiology of cirrhosis can account for the difference between the studies, as well as the high non-specific binding of ^{11}C -PK11195 in the brain and a poor signal-to-noise ratio might result in the outcome of this study [34-36]. The pilot human study by Cagnin et al [13] did not have histopathological studies as reference standard to evaluate neuroinflammation status. One recent study supported our findings of ^{11}C -PK11195, in which Bartels et al [37] found no difference of binding potential of ^{11}C -PK11195 between patients with Parkinson disease and controls. To our knowledge, there have been no reports which used ^{11}C -PK11195 PET to image neuroinflammation in HE animal model.

Our study showed that ^{18}F -DPA-714 might be more suitable for neuroinflammation imaging in chronic HE rats compared with ^{11}C -PK11195, which was consistent with several previous ^{18}F -DPA-714 studies in animal models of acute neuroinflammation

and cerebral ischemia [18, 19, 32, 38] and the regional brain predominance of neuroinflammation was also supported by several other studies with other PET techniques [2, 6, 39]. For example, Chauveau et al [18] found ^{18}F -DPA-714 performed better than ^{11}C -PK11195 to detect neuroinflammation in the rat model with intrastriatal injection of (R,S)-alpha-amino-3-hydroxy-5-methyl-4-isoxazolopropionate, which can cause a strong neuroinflammatory response. Macdonald et al [39] using ^{11}C -flumazenil PET study in 9 recurrent HE patients found significantly increased binding in the thalamus, cerebellum, and pons. Thus, with the potentially wide clinical use due to the ^{18}F PET isotope, ^{18}F -DPA-714 appears to be a promising alternative to ^{11}C -PK11195.

To demonstrate the potential of ^{18}F -DPA-714 in imaging neuroinflammation of chronic HE, we evaluated IBU treatment response of neuroinflammation in chronic HE by using ^{18}F -DPA-714. We found that both BDL and BDL+HD administration induced the same behavioral and inflammatory factors, indicating that either the BDL+HD or BDL procedure are feasible in establishing HE models to investigate neuroinflammation in chronic HE. IBU was not shown to affect blood ammonia level or chronic liver failure in HE models, however IBU can restore motor function, including motor activity, motor coordination, and tolerance. It has also been observed by CD11b immunohistochemistry that IBU can reverse microglia activation and inhibit the inflammatory markers of HE rats. ^{18}F -DPA-714 PET imaging supported the above mentioned findings. Interestingly, BDL+IBU rats showed significantly lower global brain radiotracer uptake values than BDL+HD+IBU rats, which requires further research. Our findings were supported by Agusti et al's study [6]. They found kinase p38, the inhibitor of mitogen-activated protein, could reduce microglial activation and levels of inflammatory markers in minimal HE rat model following PCS. Thus, it is possible to monitor anti-neuroinflammation treatment efficiency by using ^{18}F -DPA-714 PET imaging.

Our study also supported the dominant distribution of neuroinflammation in chronic HE. The average % ID/g values of several regional brains had significant differences among each group. These brain regions involved the basal ganglia-thalamus-cortical circuit, which was markedly connected to cognitive function [40, 41]. In a whole brain functional connectivity study of minimal HE patients, Zhang et al [40] reported that functional connectivity impairment in the basal ganglia-thalamocortical circuit could play an important role in mediating

neurocognitive dysfunction, especially for psychomotor speed and attention deficits in patients with minimal HE. The present study showed abnormal radiotracer uptake, indicating neuroinflammation was present in this circuit of HE. We also found other brain regions, mainly connecting to behavior alteration, were affected, including motor cortex, somatosensory cortex, cerebellum, and so on, showed significant differences among the groups. These findings were shown in previous studies [6, 41]. Dhanda et al [41] reported that disturbed dopaminergic and serotonergic pathways in hippocampus, striatum and cerebellum regions were responsible for behavioral impairments. Thus, neuroinflammation might contribute to the behavioral changes seen in HE when viewed from a pathophysiological perspective.

Some limitations should be acknowledged in the present study. First, our results are limited to a small number of animals in each group due to the high cost of PET and mortality of the BDL rats. Second, attenuation and scatter correction were not performed because only PET was acquired. Further studies are needed to validate our findings in this study. Third, neuroinflammation is not specific to HE, nor is TSPO expressed solely on activated microglia [42], lack indicators of TSPO quantification, and further imaging studies should be initiated in HE models or patients using other potential markers of neuroinflammation. Fourth, this study lacked a water maze or Y maze to evaluate the learning abilities of the rats, which needs further investigation. Fifth, only CD11b staining was performed to visualize microglia in this study, other microglia markers should be quantified in future studies. Sixth, the cytokines levels showed positive correlation with uptake values of ^{18}F -DPA-714, which indicates that systemic inflammation was related to neuroinflammation [1]. Further study is needed to exclude the influence of inflammatory conditions such as abdominal inflammation. Finally, our study results cannot be generalized to other HE types such as acute or chronic HE.

In conclusion, our study shows ^{18}F -DPA-714 is a more sensitive radiotracer for neuroinflammation imaging of chronic HE compared to ^{11}C -PK11195. ^{18}F -DPA-714 PET imaging can quantitatively evaluate the neuroinflammation load and distribution which are correlated with behavioral changes. This study also found that ^{18}F -DPA-714 PET imaging can assess therapeutic effectiveness of anti-neuroinflammation drugs. Thus, ^{18}F -DPA-714 PET imaging shows a promising potential to investigate neuroinflammation in chronic HE for further clinical studies.

Supplementary Material

Supplementary tables and figures.

<http://www.thno.org/v06p1220s1.pdf>

Abbreviations

HE: hepatic encephalopathy; TSPO: translocator protein; BDL: bile duct ligation; HD: hyperammonemic diet; IBU: Ibuprofen; NS: normal saline; PCS: portacaval shunt; PET: positron emission tomography; ROI: regions of interest; %ID/g: presented as percent injected dose per gram; ALT: alanine aminotransferase; AST: aspartate transaminase; EDTA: ethylene diamine tetraacetic acid; IL: interleukin; TNF- α : tumor necrosis factor alpha; ELISA: enzyme-linked immune sorbent assay; PBS: phosphate buffered saline; H&E: hematoxylin-eosin; SD: standard deviation; ANOVA: analysis of variance.

Acknowledgement

This work was supported by grants from National Natural Science Foundation of China (grants No. 81322020, 81230032, and 81171313 to L.J.Z.) and the Program for New Century Excellent Talents in the University (NCET-12-0260).

Conflicts of Interest

All authors have no conflict of interest to declare.

References

- Butterworth RF. The liver-brain axis in liver failure: neuroinflammation and encephalopathy. *Nat Rev Gastroenterol Hepatol*. 2013; 10:522-8.
- Rodrigo R, Cauli O, Gomez-Pinedo U, Agusti A, Hernandez-Rabaza V, Garcia-Verdugo JM, et al. Hyperammonemia induces neuroinflammation that contributes to cognitive impairment in rats with hepatic encephalopathy. *Gastroenterology*. 2010; 139:675-84.
- Felipo V. Hepatic encephalopathy: effects of liver failure on brain function. *Nat Rev Neurosci*. 2013; 14:851-8.
- Glass CK, Saijo K, Winner B, Marchetto MC, Gage FH. Mechanisms underlying inflammation in neurodegeneration. *Cell*. 2010; 140:918-34.
- Heneka MT, Carson MJ, El Khoury J, Landreth GE, Brosseron F, Feinstein DL, et al. Neuroinflammation in Alzheimer's disease. *Lancet Neuro*. 2015; 14:388-405.
- Agusti A, Dziedzic JL, Hernandez-Rabaza V, Guilarte TR, Felipo V. Rats with minimal hepatic encephalopathy due to portacaval shunt show differential increase of translocator protein (18 kDa) binding in different brain areas, which is not affected by chronic MAP-kinase p38 inhibition. *Metab Brain Dis*. 2014; 29:955-63.
- Rupprecht R, Papadopoulos V, Rammes G, Baghai TC, Fan J, Akula N, et al. Translocator protein (18 kDa) (TSPO) as a therapeutic target for neurological and psychiatric disorders. *Nat Rev Drug Discov*. 2010; 9:971-88.
- Rupprecht R, Rammes G, Eser D, Baghai TC, Schüle C, Nothdurfter C, et al. Translocator protein (18 kDa) as target for anxiolytics without benzodiazepine-like side effects. *Science*. 2009; 325:490-3.
- Chen MK, Guilarte TR. Translocator protein 18 kDa (TSPO): molecular sensor of brain injury and repair. *Pharmacol Ther*. 2008; 118:1-17.
- Thiel A, Heiss WD. Imaging of microglia activation in stroke. *Stroke*. 2011; 42:507-12.
- Dickens AM, Vainio S, Marjamäki P, Johansson J, Lehtiniemi P, Rokka J, et al. Detection of microglial activation in an acute model of neuroinflammation using PET and radiotracers ^{11}C -(R)-PK11195 and ^{18}F -GE-180. *J Nucl Med*. 2014; 55:466-72.
- Garvey LJ, Pavese N, Politis M, Ramlackhansingh A, Brooks DJ, Taylor-Robinson SD, et al. Increased microglia activation in neurologically asymptomatic HIV-infected patients receiving effective ART. *AIDS*. 2014; 28:67-72.
- Cagnin A, Taylor-Robinson SD, Forton DM, Banati RB. In vivo imaging of cerebral "peripheral benzodiazepine binding sites" in patients with hepatic encephalopathy. *Gut*. 2006; 55:547-53.
- Desjardins P, Butterworth RF. The "peripheral-type" benzodiazepine (omega 3) receptor in hyperammonemic disorders. *Neurochem Int*. 2002; 41:109-14.
- Lavoie J, Layrargues GP, Butterworth RF. Increased densities of peripheral-type benzodiazepine receptors in brain autopsy samples from cirrhotic patients with hepatic encephalopathy. *Hepatology*. 1990; 11:874-8.
- Banati RB. Visualising microglial activation in vivo. *Glia*. 2002; 40:206-17.
- Kropholler MA, Boellaard R, van Berckel BN, Schuitemaker A, Kloet RW, Lubberink MJ, et al. Evaluation of reference regions for (R)-[^{11}C]PK11195 studies in Alzheimer's disease and mild cognitive impairment. *J Cereb Blood Flow Metab*. 2007; 27:1965-74.
- Chauveau F, Van Camp N, Dollé F, Kuhnast B, Hinnen F, Damont A, et al. Comparative evaluation of the translocator protein radioligands ^{11}C -DPA-713, ^{18}F -DPA-714, and ^{11}C -PK11195 in a rat model of acute neuroinflammation. *J Nucl Med*. 2009; 50:468-76.
- Lavis S, Inoue K, Jan C, Peyronneau MA, Petit F, Goutal S, et al. [^{18}F]DPA-714 PET imaging of translocator protein TSPO (18 kDa) in the normal and excitotoxically-lesioned nonhuman primate brain. *Eur J Nucl Med Mol Imaging*. 2015; 42:478-94.
- Wang Y, Yue X, Kiesewetter DO, Wang Z, Lu J, Niu G, et al. [^{18}F]DPA-714 PET imaging of AMD3100 treatment in a mouse model of stroke. *Mol Pharm*. 2014; 11:3463-70.
- Jover R, Rodrigo R, Felipo V, Insausti R, Sáez-Valero J, García-Ayllón MS, et al. Brain edema and inflammatory activation in bile duct ligated rats with diet-induced hyperammonemia: A model of hepatic encephalopathy in cirrhosis. *Hepatology*. 2006; 43:1257-66.
- Wang YX, Yuan J, Chu ES, Go MY, Huang H, Ahuja AT, et al. T1rho MR imaging is sensitive to evaluate liver fibrosis: an experimental study in a rat biliary duct ligation model. *Radiology*. 2011; 259:712-9.
- Semon BA, Leung PM, Rogers QR, Gietzen DW. Plasma ammonia, plasma, brain and liver amino acids and urea cycle enzyme activities in rats fed ammonium acetate. *J Nutr*. 1989; 119:166-74.
- Chen JR, Wang BN, Tseng GF, Wang YJ, Huang YS, Wang TJ. Morphological changes of cortical pyramidal neurons in hepatic encephalopathy. *BMC Neurosci*. 2014; 15:15.
- Azorín I, Miñana MD, Felipo V, Grisolia S. A simple animal model of hyperammonemia. *Hepatology*. 1989; 10:311-4.
- Cauli O, Rodrigo R, Piedrafita B, Boix J, Felipo V. Inflammation and hepatic encephalopathy: Ibuprofen restores learning ability in rats with portacaval shunts. *Hepatology*. 2007; 46:514-9.
- Cauli O, Rodrigo R, Piedrafita B, Llansola M, Mansouri MT, Felipo V. Neuroinflammation contributes to hypokinesia in rats with hepatic encephalopathy: ibuprofen restores its motor activity. *J Neurosci Res*. 2009; 87:1369-74.
- Agusti A, Cauli O, Rodrigo R, Llansola M, Hernández-Rabaza V, Felipo V. p38 MAP kinase is a therapeutic target for hepatic encephalopathy in rats with portacaval shunts. *Gut*. 2011; 60:1572-9.
- Tomasi G, Edison P, Bertoldo A, Roncaroli F, Singh P, Gerhard A, et al. Novel reference region model reveals increased microglial and reduced vascular binding of ^{11}C -(R)-PK11195 in patients with Alzheimer's disease. *J Nucl Med*. 2008; 49:1249-56.
- Pugliese F, Gaemperli O, Kinderlerer AR, Lamare F, Shalhoub J, Davies AH, et al. Imaging of vascular inflammation with [^{11}C]PK11195 and positron emission tomography/computed tomography angiography. *J Am Coll Cardiol*. 2010; 56:653-61.
- Golla SS, Boellaard R, Oikonen V, Hoffmann A, van Berckel BN, Windhorst AD, et al. Quantification of [^{18}F]DPA-714 binding in the human brain: initial studies in healthy controls and Alzheimer's disease patients. *J Cereb Blood Flow Metab*. 2015; 35:766-72.
- James ML, Fulton RR, Vercoullie J, Henderson DJ, Garreau L, Chalon S, et al. DPA-714, a new translocator protein-specific ligand: synthesis, radiofluorination, and pharmacologic characterization. *J Nucl Med*. 2008; 49:814-22.
- Visser EP, Disselhorst JA, Brom M, Laverman P, Gotthardt M, Oyen WJ, et al. Spatial resolution and sensitivity of the Inveon small-animal PET scanner. *J Nucl Med*. 2009; 50:139-47.
- Venneti S, Lopresti BJ, Wiley CA. Molecular imaging of microglia/macrophages in the brain. *Glia*. 2013; 61:10-23.
- Su YY, Yang GF, Lu GM, Wu S, Zhang LJ. PET and MR imaging of neuroinflammation in hepatic encephalopathy. *Metab Brain Dis*. 2015; 30:31-45.
- Mach RH. New targets for the development of PET tracers for imaging neurodegeneration in Alzheimer disease. *J Nucl Med*. 2014; 55:1221-4.
- Bartels AL, Willemsen AT, Doorduyn J, de Vries EF, Dierckx RA, Leenders KL. [^{11}C]PK11195 PET: quantification of neuroinflammation and a monitor of anti-inflammatory treatment in Parkinson's disease? *Parkinsonism Relat Disord*. 2010; 16:57-9.
- Boutin H, Prenant C, Maroy R, Galea J, Greenhalgh AD, Smigova A, et al. [^{18}F]DPA-714: direct comparison with [^{11}C]PK11195 in a model of cerebral ischemia in rats. *PLoS One*. 2013; 8:e56441.
- Macdonald GA, Frey KA, Agranoff BW, Minoshima S, Koeppe RA, Kuhl DE, et al. Cerebral benzodiazepine receptor binding in vivo in patients with recurrent hepatic encephalopathy. *Hepatology*. 1997; 26:277-82.

40. Zhang L, Qi R, Wu S, Zhong J, Zhong Y, Zhang Z, et al. Brain default-mode network abnormalities in hepatic encephalopathy: a resting-state functional MRI study. *Hum Brain Mapp.* 2012; 33:1384-92.
41. Dhanda S, Sandhir R. Role of dopaminergic and serotonergic neurotransmitters in behavioral alterations observed in rodent model of hepatic encephalopathy. *Behav Brain Res.* 2015; 286:222-35.
42. Berding G, Banati RB, Buchert R, Chierichetti F, Grover VP, Kato A, et al. Radiotracer imaging studies in hepatic encephalopathy: ISHEN practice guidelines. *Liver Int.* 2009; 29:621-8.